Supplementary Information

Selective Control of Sharp-Edge Zinc Electrodes with (002) Plane for High-Performance Aqueous Zinc-Ion Batteries

Hee Bin Jeong,[1,†] Dong Il Kim,[1,†] Geun Yoo,[2,†] Dasari Mohan,[1] Arijit Roy,[1] Min Jung,[3] Hyeong Seop Jeong,[1] SeungNam Cha,[3] Geon Hyoung An,[2,*] Pil-Ryung Cha,[1,**] and John Hong[1,***]

[1]School of Materials Science and Engineering, Kookmin University, 77 Jeongneung-ro, Seongbuk-gu, Seoul, 02707, Republic of Korea

[2]Department of Energy System Engineering, Gyeongsang National University, 33 Dongjin-ro, Jinju, Gyeongnam 52828, Republic of Korea

[3]Department of Physics, Sungkyunkwan University, 2066 Seobu-ro, Jangan-gu, Suwon-si, Gyeonggi-do 16419, Republic of Korea

*Correspondence: ghan@gnu.ac.kr

**Correspondence: cprdream@kookmin.ac.kr

***Correspondence: johnhong@kookmin.ac.kr

†These authors contributed equally.

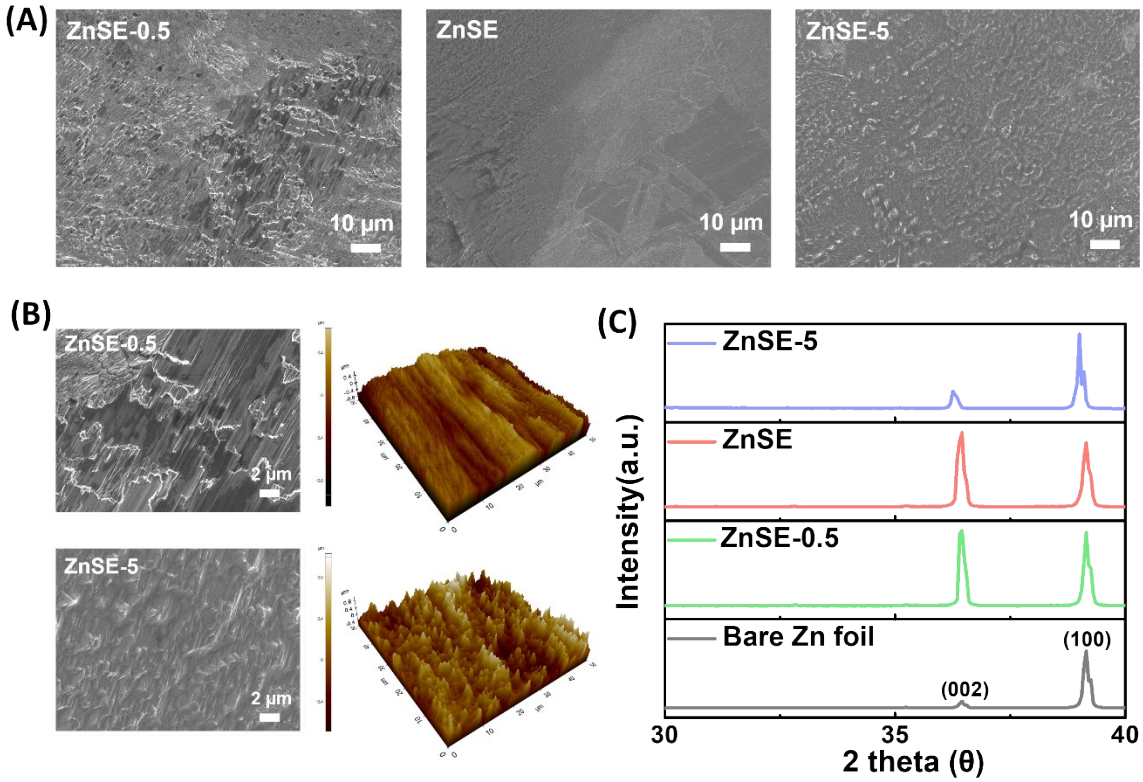

Figure S1. (A) Low-magnification surface SEM images of ZnSE-0.5, ZnSE, and ZnSE-5. (B) Surface SEM images, and 3D-AFM images of ZnSE-0.5 and ZnSE-5. (C) XRD patterns of the bare Zn foil, ZnSE-0.5, ZnSE, and ZnSE-5.

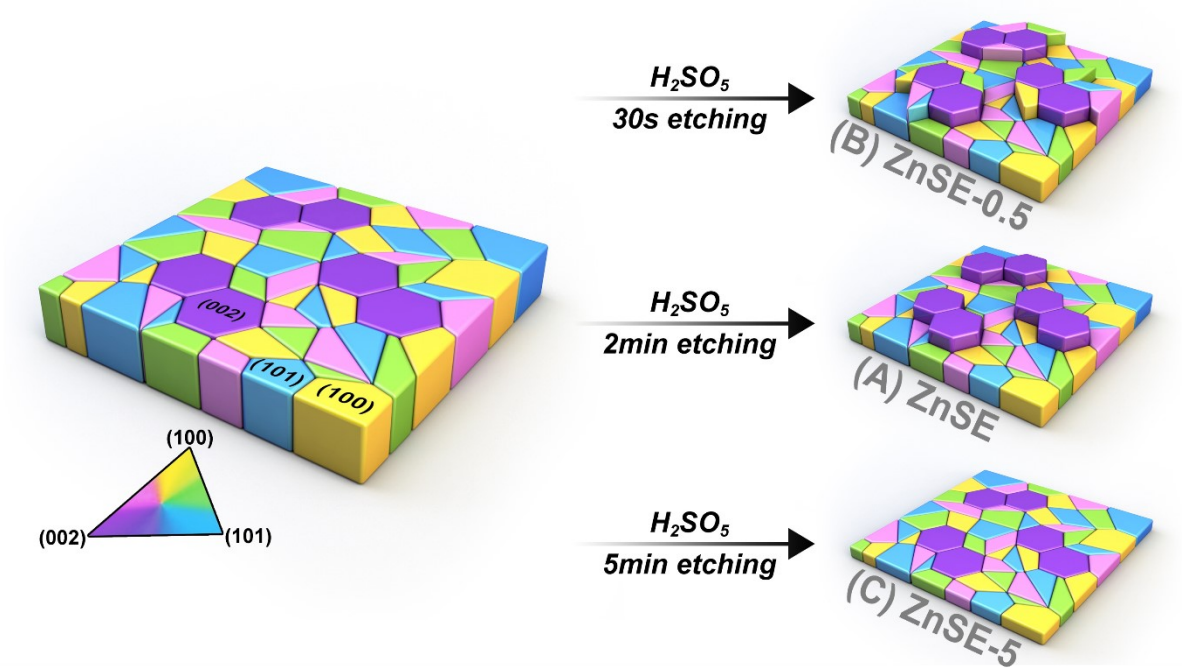

Figure S2. Schematic illustration of ZnSE, ZnSE-0.5, and ZnSE-5: (A) the (002)-dominated Zn foil (ZnSE) for 2-min etching, (B) the partial (002)-dominated Zn foil for 30-s etching (ZnSE-0.5), and (C) the (002)-nondominated Zn foil for 5-min etching (ZnSE-5)).

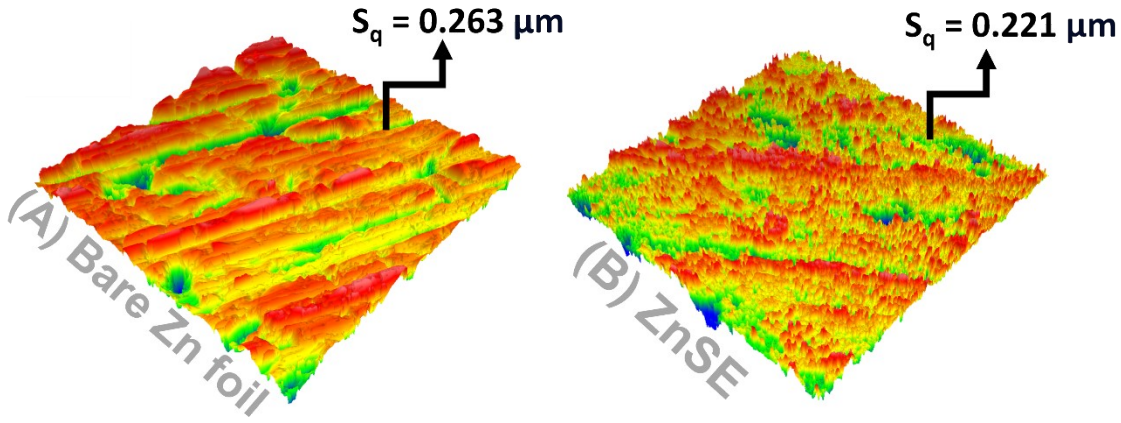

Figure S3. Coherence scanning interferometric (CSI) profiler images of the (A) bare Zn foil and (B) ZnSE.

\

Figure S4. Contact angles of deionized water on the surfaces of the bare Zn foil and ZnSE.

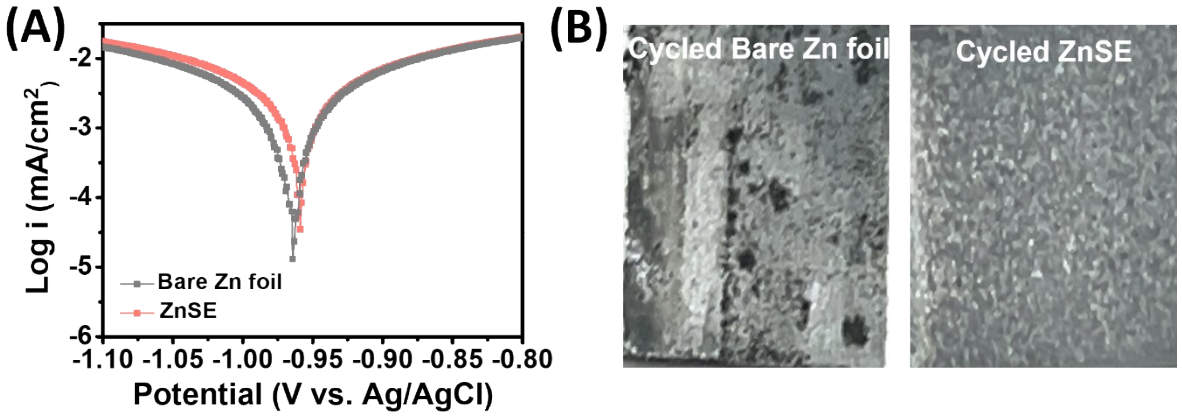

Figure S5. (A) Tafel plots for describing the corrosion of the bare Zn foil and ZnSE. (B) Optical images of the bare Zn foil and ZnSE after the electrochemical cycling.

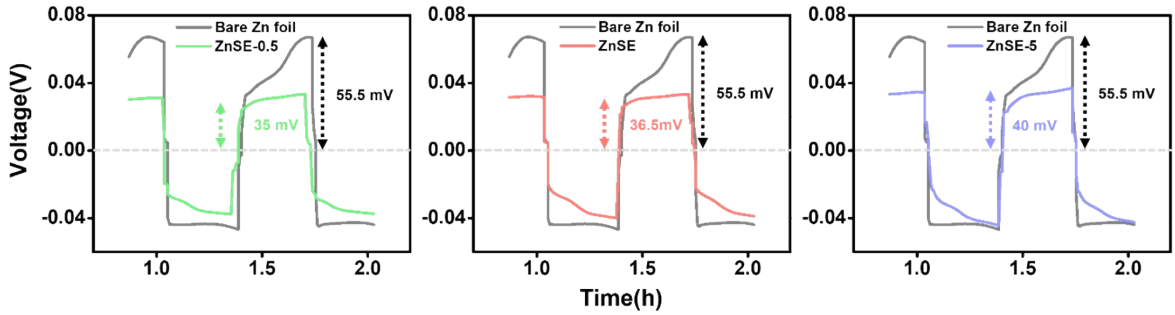

Figure S6. Overpotential of the symmetric Zn||Zn cells at the current density of 3 mA/cm^2 and the capacity of 1 mAh/cm^2 for the bare Zn foil, ZnSE-0.5, ZnSE, and ZnSE-5.

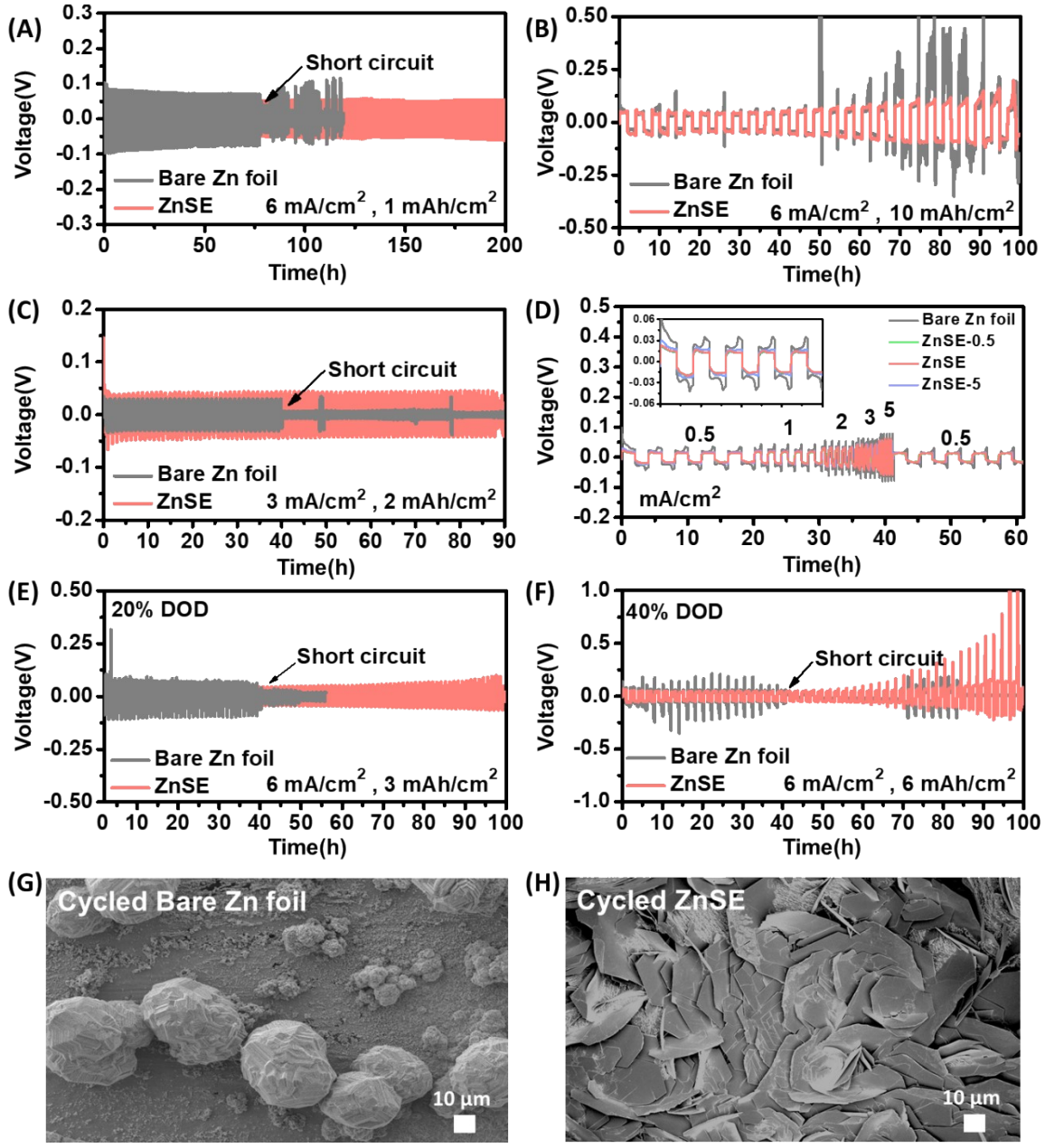

Figure S7. Voltage profile of the symmetric Zn||Zn cells for the bare Zn foil and ZnSE from the Zn foil with a thickness of 50 μm (A) at the current density of 6 mA/cm^2 and the capacity of 1 mAh/cm^2 and (B) at the current density of 6 mA/cm^2 and the capacity of 10 mAh/cm^2 (C) at the current density of 3 mA/cm^2 and the capacity of 2 mAh/cm^2 for the comparison. (D) voltage profile of the symmetric Zn||Zn cells for the bare Zn foil and ZnSE at the different current densities by applying the different etching time. Voltage profile of the symmetric Zn||Zn cells for the bare Zn foil and ZnSE cells under different current densities and areal

capacities: (E) at 6 mA/cm^2 and 3 mAh/cm^2 (20% DOD), (F) at 6 mA/cm^2 and 6 mAh/cm^2 (40% DOD). Low magnification surface SEM images of the (G) bare Zn foil and (H) ZnSE after 20 h of cycling.

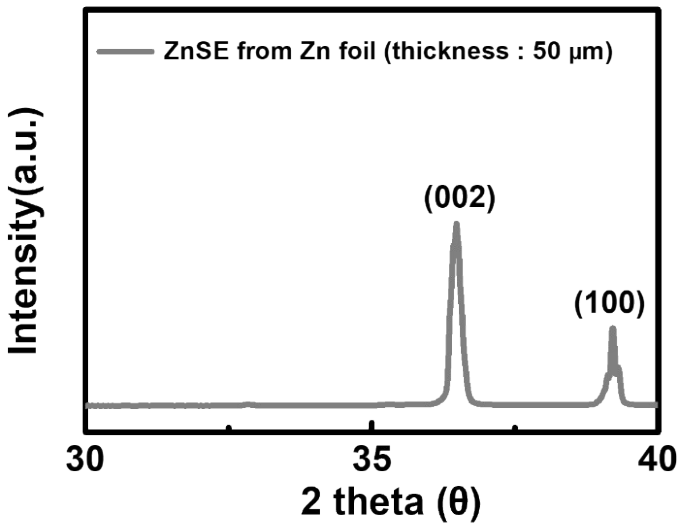

Figure S8. XRD patterns of the ZnSE from the Zn foil with a thickness of 50 μm

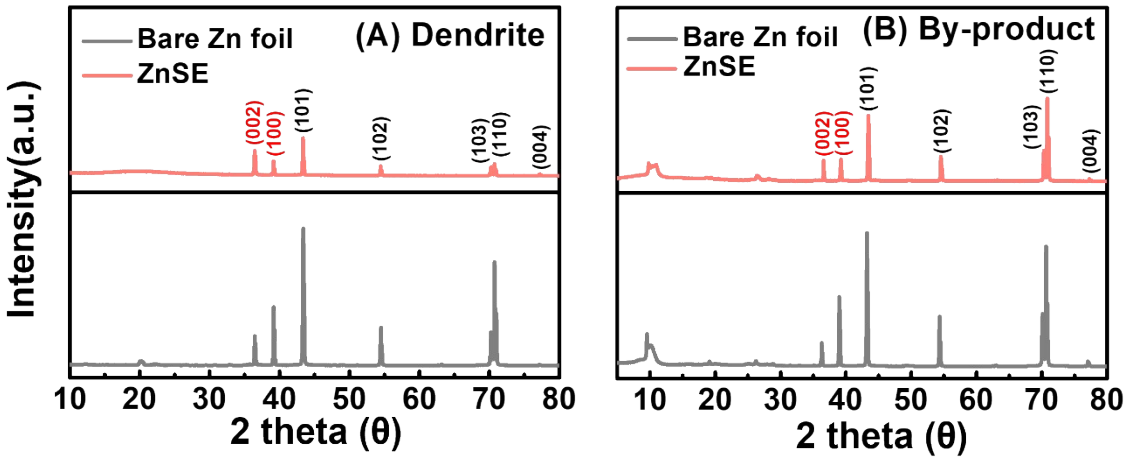

Figure S9. XRD patterns of the bare Zn foil and ZnSE (A) after the electrochemical dendrite test for 20 h and (B) after the by-product test.

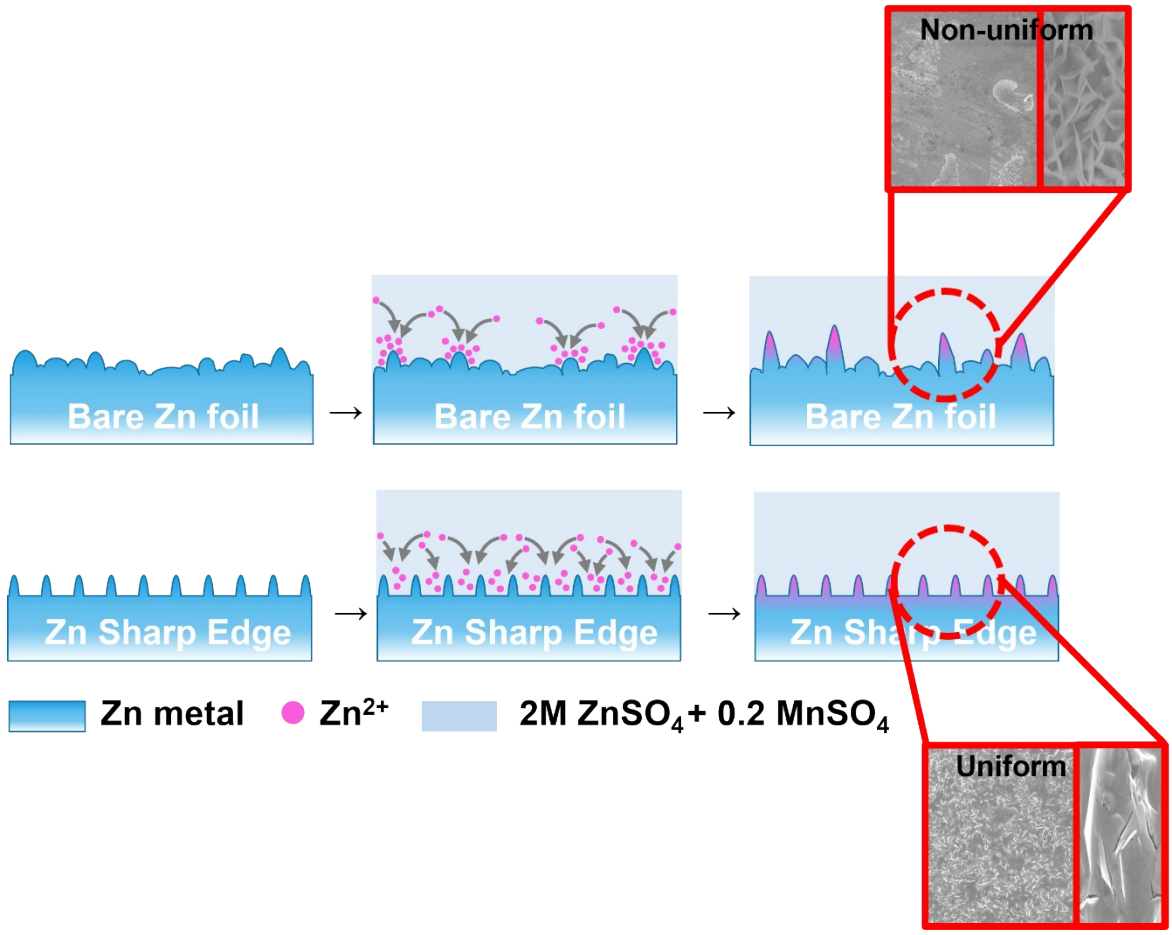

Figure S10. Schematic of the Zn plating process on the bare Zn foil and ZnSE electrode.

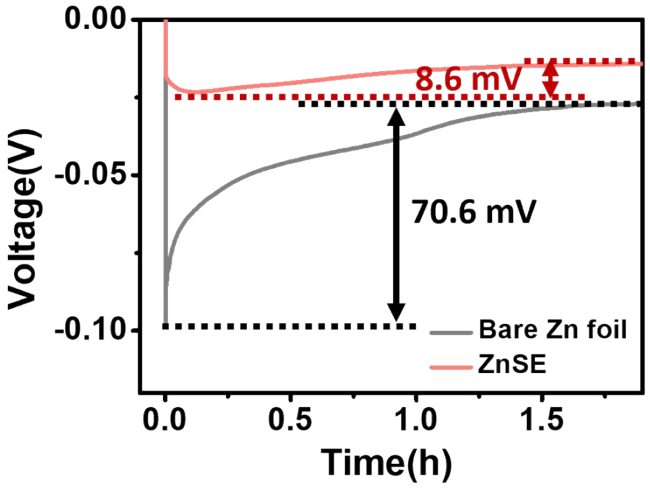

Figure S11. Nucleation overpotential curves for the bare Zn foil and ZnSE.

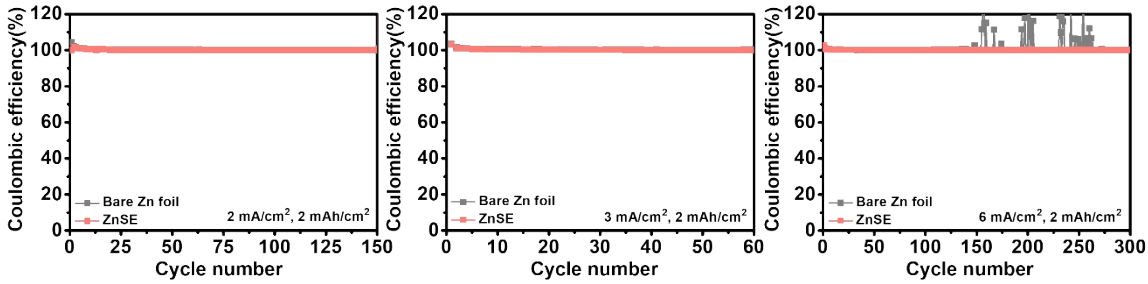

Figure S12. Columbic efficiency of the asymmetric cell at current densities of 2, 3, 6 mA/cm^2 and the capacity of 2 mAh/cm^2.

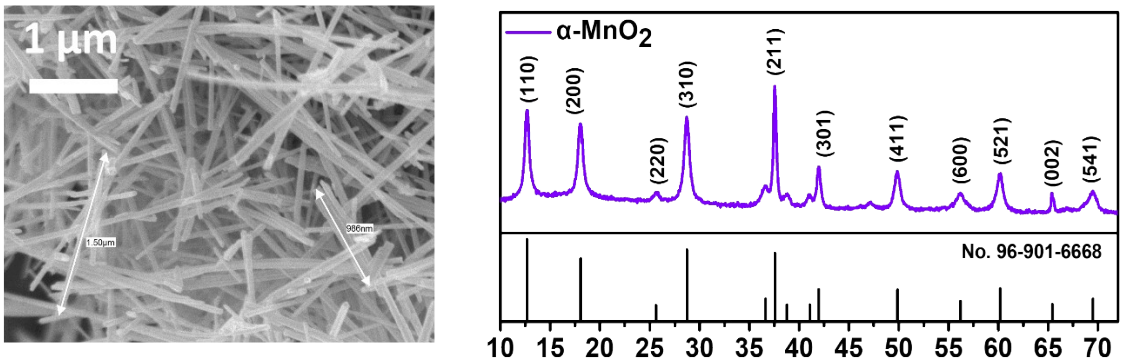

Figure S13. XRD pattern and SEM image of the α-MnO2 electrode produced by the hydrothermal synthesis.

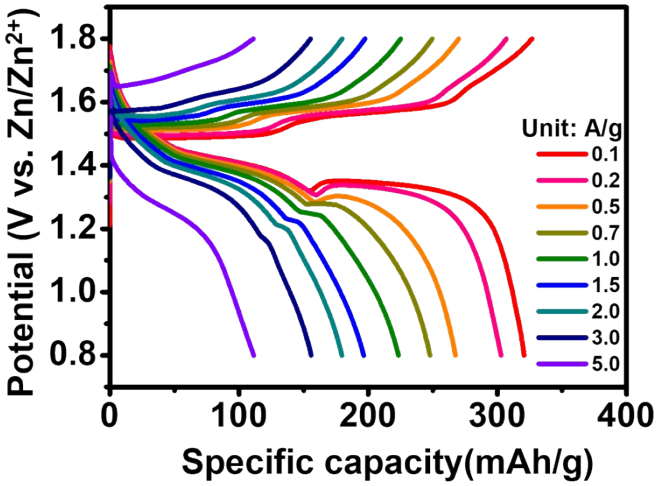

Figure S14. GCD profile of the ZnSE electrode at different current densities.

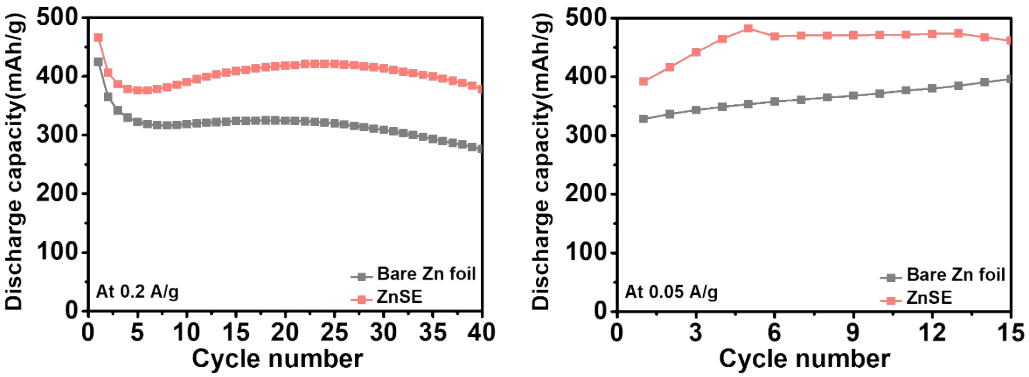

Figure S15. Early cycling performance of the bare Zn foil and ZnSE at low current densities of 0.2 and 0.05A/g.

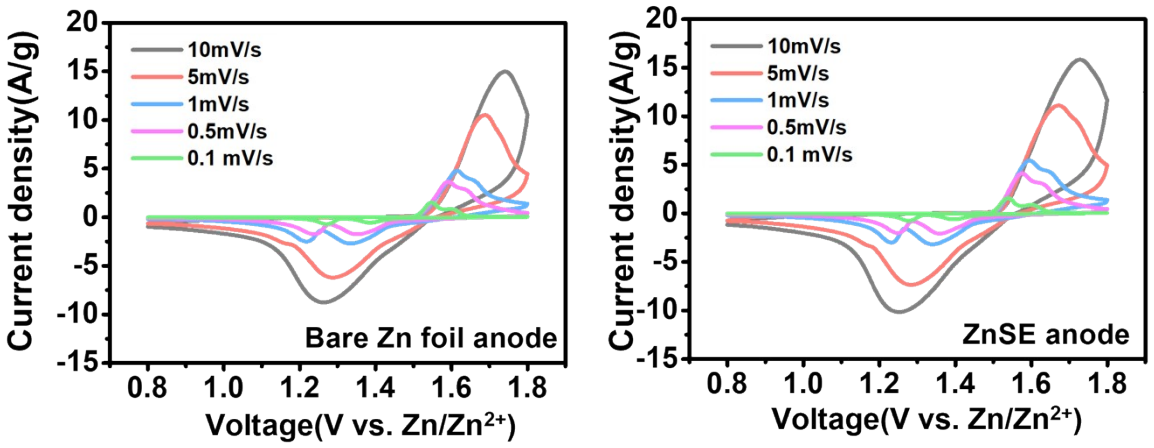

Figure S16. CV curves of the bare Zn foil and ZnSE electrode at different scan rates.

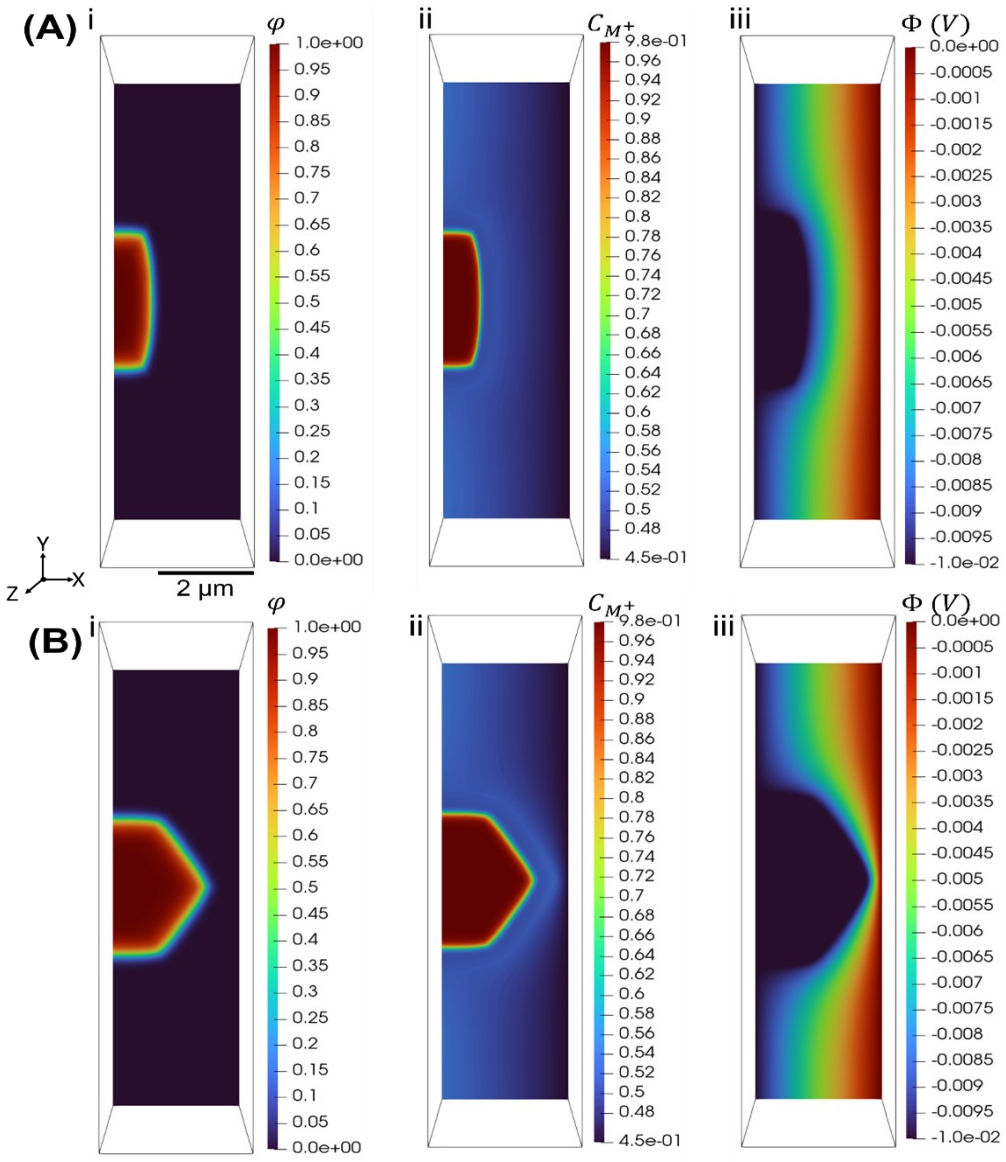

Figure S17. 2D cross section view at mid-plane of simulation domain along Z-axis for (A) θ = 0° and (B) θ = 90°. i, ii and iii images represent the profile distributions for phase-field order parameter, composition of Zn ions and electric potentials, respectively.

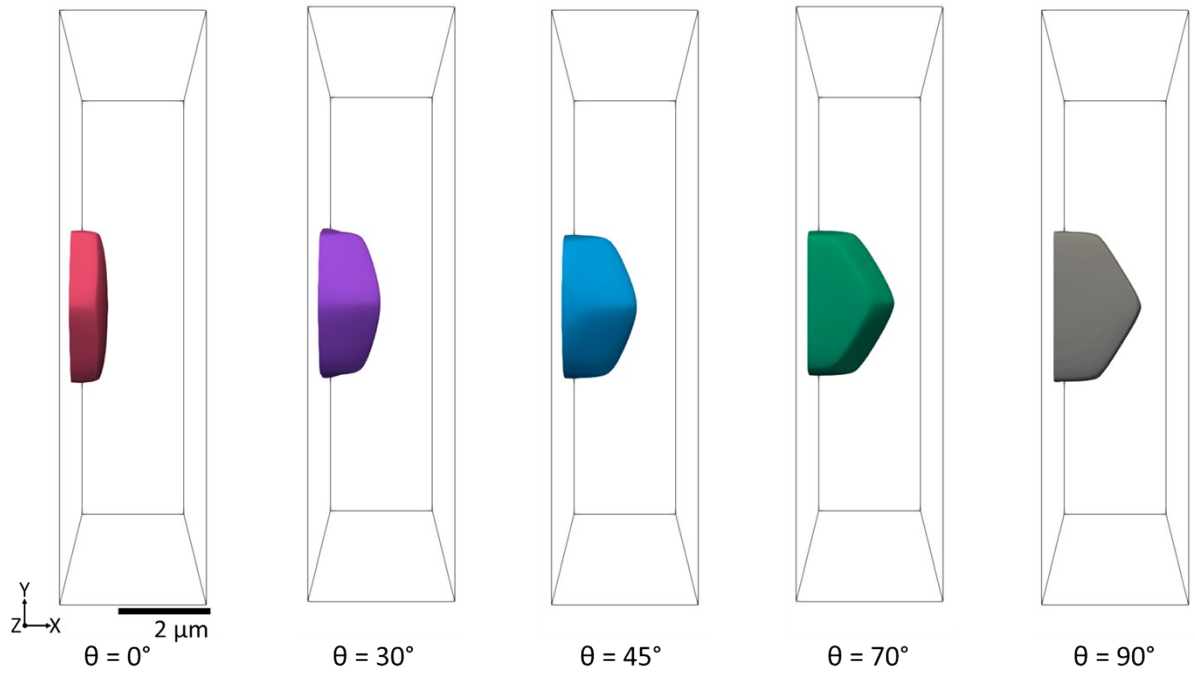

Figure S18. Growth morphology as function of [002] direction orientation with X-axis. The figures represent the iso-surface of φ at 0.5.

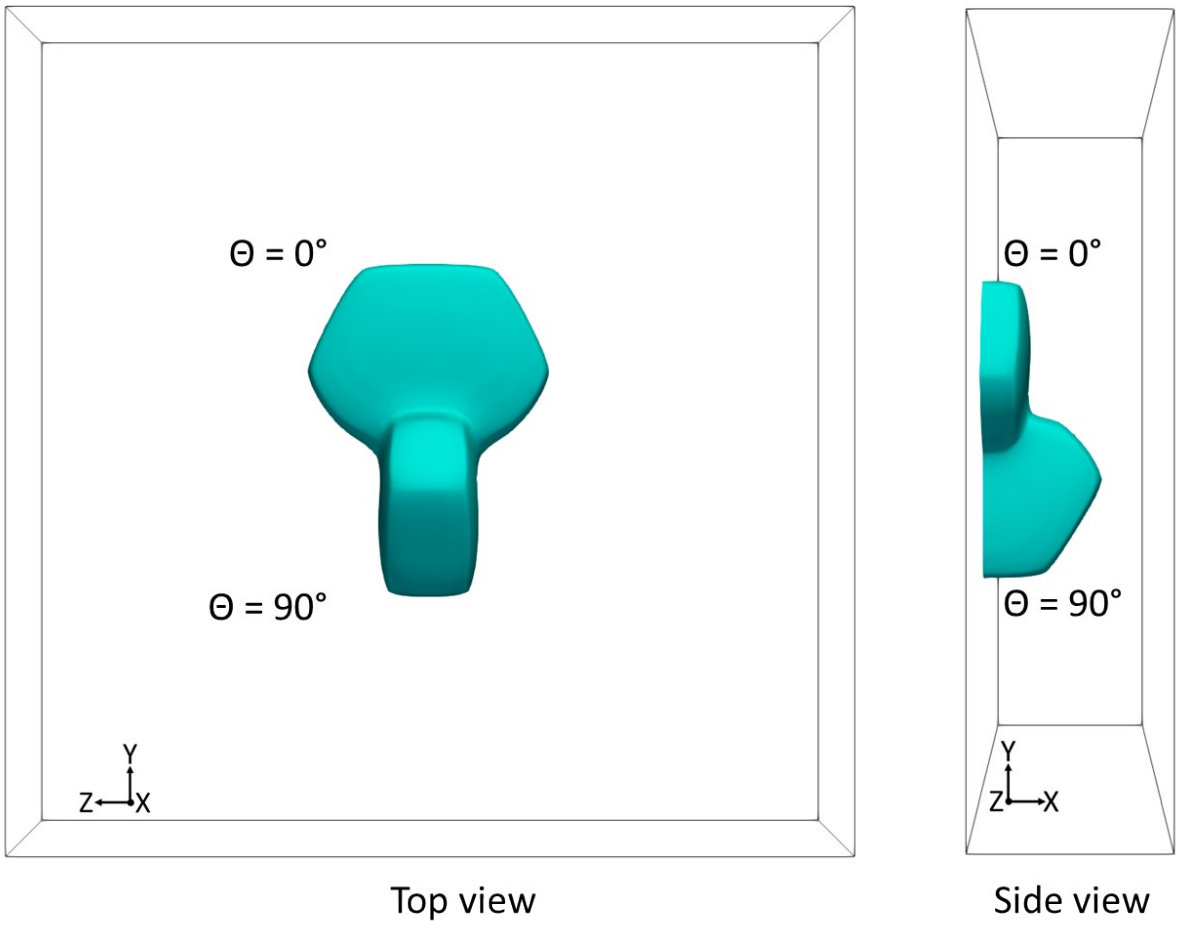

Figure S19. Phase-field iso-surface at φ = 0.5 for two orientations growth during electrodeposition under external electric potential.

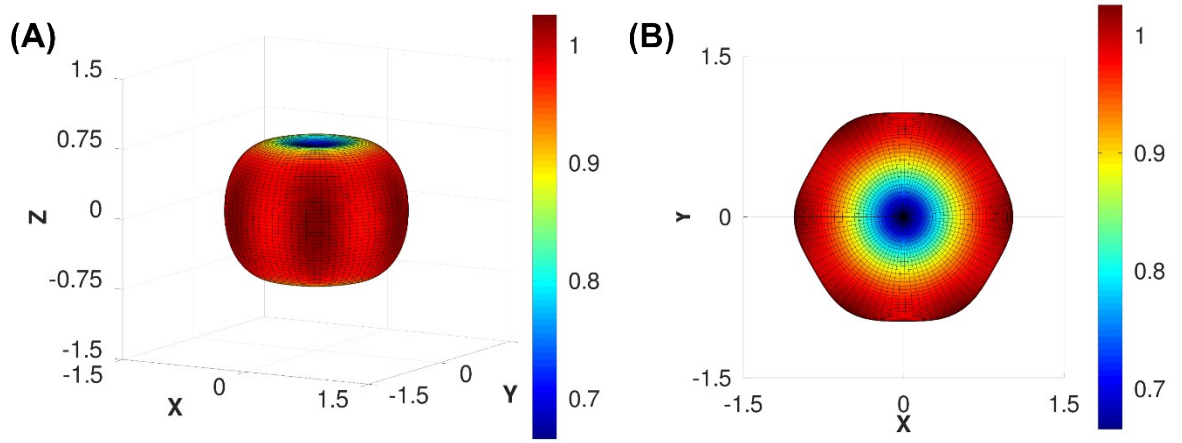

Figure S20. 3D polar plot of anisotropy function (A) arbitrary view and (B) view along Z-direction ([002] direction)

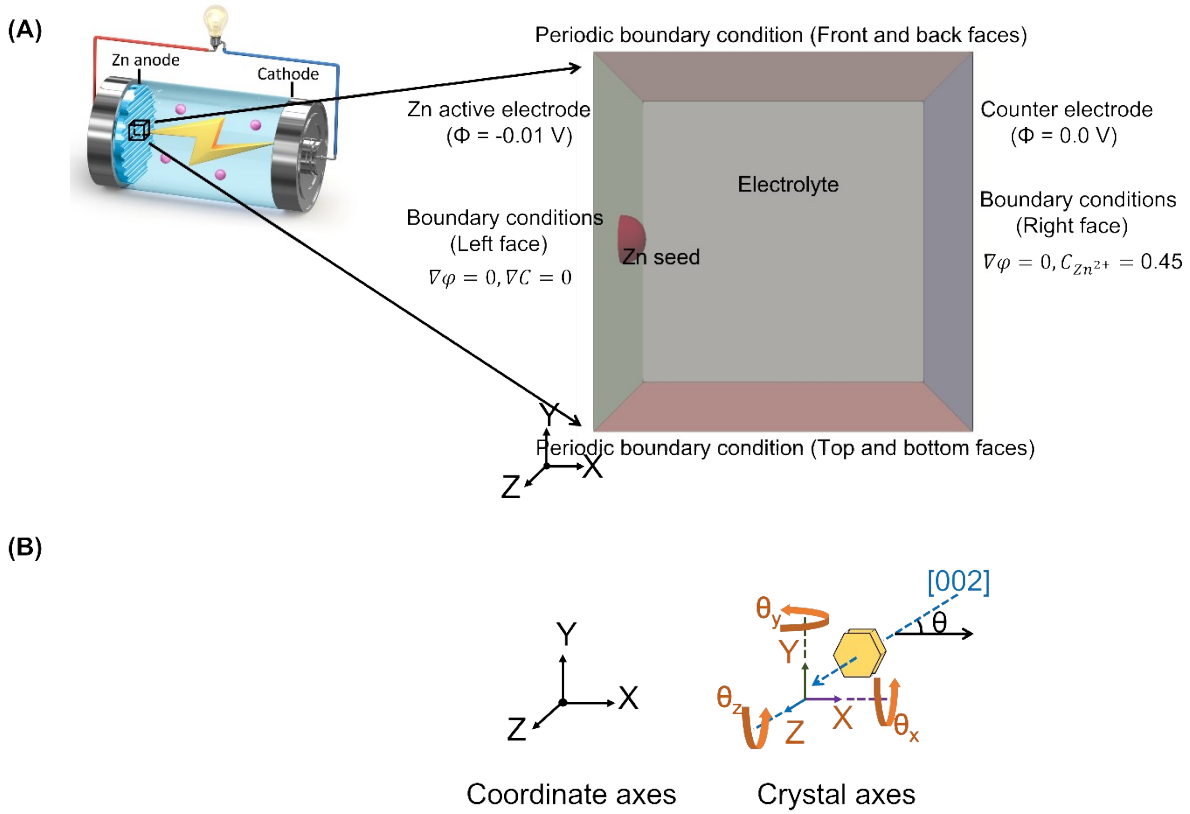

Figure S21. (A) Schematic of phase-field simulation domain represents the initial seed and boundary conditions. Left side (at X = 0, YZ plane, green colour) is active Zn anode and right side (violet colour) is counter electrode. (B) Schematic of axes, representing the relation between external coordinate axes and crystal axes. θ_x, θ_y, θ_z represents the rotations about X, Y and Z-axis, respectively. θ represents angle between external coordinate X-axis and [002] plane of the Zn crystal. The figure is for illustration only and the structural details are not to scale.

Strategy	Etching time	Etchant	Symmetrical cell	Ref
ZnSE	2min	piranha solution	14 mV (1 mA /cm^2 and 1 mA h/cm^2) 53 mV (5 mA /cm^2 and 1 mA h/cm^2)	This work
r-Zn	5min	dilute hydrochloric acid solution (6 vol %)	20 mV (1 mA /cm^2 and 0.5 mA h/cm^2)	Ref.1
TFA-AN@Zn	24h	trifluoromethanesulfonic acid (TFA) in acetonitrile (AN)	50 mV (4 mA /cm^2 and 2mA h /cm^2)	Ref.2
PPZ@Zn	4min	phosphoric acid	29.1 mV (1 mA /cm^2 and 1 mA h /cm^2)	Ref.3
h-Zn	4 – 8min	dilute phosphoric acid(H_3PO4)	80 mV (5 mA /cm^2 and 1 mA h /cm^2)	Ref.4
TA@Zn	3 – 9min	tartaric acid	89 mV (5 mA /cm^2 and 1 mA h /cm^2)	Ref.5
ZnSA	10min	concentrated phosphoric acid (H_3PO_4, 85%)	69 mV (5 mA /cm^2 and 2 mA h /cm^2)	Ref.6
3D Zn anode	15h	5 wt % $NH_3{\cdot}H_2O$ solution	20 mV (0.5 mA /cm^2 and 0.5 mA h /cm^2)	Ref.7
DCP-Zn	30min	H_3PO_4 solution	60 mV (0.5 mA /cm^2 and 0.1 mA h /cm^2)	Ref.8

Table S1. Comparison of the synthetic and electrochemical parameters of the ZnSE electrode with the results of other studies.

Anode	Cathode	Electrolyte	Retention	Performance	Ref
Zn foil	α-MnO_2	2M $ZnSO_4$ +0.2M $MnSO_4$	94% (at 0.5A/g for 300 cycle)	275 mAh/g at 0.5 A/g	This work
Zn foil	V_2O_5	4M $Zn(BF_4)_2$/EG	70% (at 0.5A/g for 300 cycle)	170 mAh/g at 0.5 A/g	Ref.9
flexible Zn	$NH_4V_3O_8$ 1.9H_2O	$ZnSO_4$/gelatin water-based QSS	95% (at 0.5A/g for 200 cycle)	400 mAh/g at 0.5 A/g	Ref.10
Zn foil	ε-MnO_2	3(21 M LiTFSI)*vs*.8(1.5 M $ZnSO_4$)	80% (at 0.5A/g for 300 cycle)	175 mAh/g at 0.5 A/g	Ref.11
Zn foil	$NH_4V_4O_{10}$	2 M $Zn(OTf)_2$ and TMU20(tetramethylurea)	68 % (at 0.5A/g for 300 cycle)	230 mAh/g at 0.5 A/g	Ref.12
Zn foil	CuO nanorods	3 M $ZnSO_4$	75% (at 0.3A/g for 200 cycle)	190 mAh/g at 0.5 A/g	Ref.13
Zn foil	$NH_4V_4O_{10}$	tannic acid (TA) and sodium alginate (SA) + 2M $ZnSO_4$	67% (at 0.5A/g for 400 cycle)	377 mAh/g at 0.5 A/g	Ref.14
Zn foil	VS_2	1M $ZnSO_4$	98% (at 0.5A/g for 200 cycle)	136 mAh/g at 0.5 A/g	Ref.15
dual-ZEI Zn/Cu	α-MnO_2	2 M $ZnSO_4$ and 0.1 M $MnSO_4$	89% (at 0.5A/g for 500 cycle)	175 mAh/g at 0.5 A/g	Ref.16
Zn foil	V/O-defected $NH_4V_4O_{10}$	3M pure $Zn(OTF)_2$ as an electrolyte	98% (at 0.5A/g for 100 cycle)	500 mAh/g at 0.5 A/g	Ref.17
Zn foil	$([N(CH_3)_4]_{0.77}$, $Zn_{0.23})$ $V_8O_{20}\cdot 3.8H_2O$	3 M $Zn(CF_3SO_3)_2$	92% (at 0.5A/g for 200 cycle)	287 mAh/g at 0.5 A/g	Ref.18
Zn foil	$Zn_\delta V_2O_5\cdot nH_2O$	3 M $Zn(CF_3SO_3)_2$	89% (at 0.5A/g for 150 cycle)	508 mAh/g at 0.5 A/g	Ref.19
Zn foil	3D spongy VO_2-graphene	2 M $Zn(CF_3SO_3)_2$	88% (at 0.5A/g for 200 cycle)	442 mAh/g at 0.5 A/g	Ref.20
zinc plate	$Na_{0.56}V_2O_5$ nanobelt	3M $ZnSO_4$ and 0.1/0.5/1 M Na_2SO_4	84% (at 0.5A/g for 200 cycle)	170 mAh/g at 0.5 A/g	Ref.21
Zn plate	Fe-doped vanadium oxide	3 M $Zn(CF_3SO_3)_2$	94% (at 0.5A/g for 300 cycle)	283 mAh/g at 0.5 A/g	Ref.22
Zn foil	MnO@N-doped graphene scrolls	2 M $ZnSO_4$ + 0.2 M $MnSO_4$	98% (at 0.5A/g for 300 cycle)	73 mAh/g at 0.5 A/g	Ref.23
Zn foil	$ZnMn_2O_4$ with conducting carbon	3 M $Zn(CF_3SO_3)_2$	94% (at 0.5A/g for 500 cycle)	90 mAh/g at 0.5 A/g	Ref.24
Zn foil	Mn_3O_4	2 M $ZnSO_4$	73% (at 0.5A/g for 300 cycle)	195 mAh/g at 0.5 A/g	Ref.25

Table S2. Comparison of the cycling electrochemical performance of the ZnSE electrode with the results of other studies.

Miller Indices	Energy (J/m^2)
(0001)	0.33
$(10\bar{1}0)$	0.53
$(10\bar{1}1)$	0.70
$(10\bar{1}2)$	0.71
$(2\bar{1}\bar{1}2)$	0.80
$(21\bar{3}0)$	0.81
$(20\bar{2}1)$	0.81
$(22\bar{4}1)$	0.83
$(21\bar{3}1)$	0.84
$(21\bar{3}2)$	0.89
$(11\bar{2}0)$	0.92
$(11\bar{2}1)$	0.93

Table S3. Theoretical surface energy of Zn.[26-27]

It has been noted that the (0001) plane exhibits the minimum energy among all crystal planes of Zn. In single-phase alloys, the etching response varies for each plane; thus, surfaces with higher energy may react to the etchant more actively due to the surface energy interaction.[28] The (0001) plane, possessing lower energy, is consequently less etched compared to planes with higher surface energy of Zn. The rate of etching in any process is predominantly determined by the duration of etching and activity of etching precursors. In the experiments, the activity of the etching precursors was carefully controlled, with the etching time being the only variable to systematically control the surface of Zn. Moreover, prolonged exposure to the etchant is well known to result in the over-etching of the material's surface. The experiments

have demonstrated that extended exposure times also lead to the etching of the (0001) planes. Therefore, we have refined the etching process to ensure a predominance of (0001) surfaces in the film.

REFERENCES (Supporting Information)

1. J. Wang, Z. Cai, R. Xiao, Y. Ou, R. Zhan, Z. Yuan and Y. Sun, *ACS Appl. Mater. Interfaces*, 2020, **12**, 23028.
2. W. Wang, G. Huang, Y. Wang, Z. Cao, L. Cavallo, M. N. Hedhili and H. N. Alshareef, *Adv. Energy Mater*., 2022, **12**, 2102797.
3. X. Wang, J. Meng, X. Lin, Y. Yang, S. Zhou, Y. Wang and A. Pan, *Adv. Fun. Mater*., 2021, **31**, 2106114.
4. Y. Zhang, X. Han, R. Liu, Z. Yang, S. Zhang, Y. Zhang and J. Sun, *Small*, 2022, **18**, 2105978
5. X. Chen, X. Shi, P. Ruan, Y. Tang, Y. Sun, W. Y. Wong, B. Lu, and J. Zhou, *Small Sci*., 2023, **3**, 2300007.
6. T. T. Su, K. Wang, B. Y. Chi, W. F. Ren and R. C. Sun, *EcoMat*, 2022, **4**, e12219.
7. Z. Kang, C. Wu, L. Dong, W. Liu, J. Mou, J. Zhang and C. Xu, *Chem. Eng*., 2019, **7**, 3364.
8. W. Guo, Z. Cong, Z. Guo, C. Chang, X. Liang, Y. Liu and X. Pu, *Energy Stor.*, *Mater*., 2020, **30**, 104.
9. Han, D., Cui, C., Zhang, K., Wang, Z., Gao, J., Guo, Y. and Yang, Q. H, *Nat. Sustain.*, 2022, 5.3: 205-213.
10. Lai, J., Tang, H., Zhu, X. and Wang, Y, *J. Mater. Chem.*, 2019, 7.40: 23140-23148.
11. Chen, Y., Gu, S., Zhou, J., Chen, X., Sun, Z., Lu, Z., and Zhang, K, *J. Alloys Compd.*, 2022, 909: 164835.
12. Li, Z., Liao, Y., Wang, Y., Cong, J., Ji, H., Huang, Z., & Huang, Y, *Energy Storage Mater.*, 2023, 56: 174-182.
13. Meng, J., Yang, Z., Chen, L., Qin, H., Cui, F., Jiang, Y. and Zeng, X, *Mater. Today Energy*, 2020, 15: 100370.

14. Zhang, B., Qin, L., Fang, Y., Chai, Y., Xie, X., Lu, B. and Zhou, J, *Science Bulletin*, 2022, 67.9: 955-962.

15. He, P., Yan, M., Zhang, G., Sun, R., Chen, L., An, Q. and Mai, L. *Adv. Energy Mater.*, 2017, 7.11: 1601920.

16. Zhu, X., Zhang, H., Wang, Z., Zhang, C., Qin, L., Chen, D. and Chen, J. *Mater. Today Energy*, 2022, 23: 100897.

17. S. Li, X. Xu, W. Chen, J. Zhao, K. Wang, J. Shen, X. Chen, X. Lu, X. Jiao, Y. Liu and Y. Bai, *Energy Storage Mater.*, 2024, **65**, 103108.

18. Li, S., Xu, X., Chen, W., Zhao, J., Wang, K., Shen, J. and Bai, Y. *Energy Storage Mater.*, 2024, 65: 103108.

19. Zhang, X., Xue, F., Sun, X., Hou, T., Xu, Z., Na, Y. and Zheng, C. *J. Chem. Eng.*, 2022, 445: 136714.

20. Luo, H., Wang, B., Wu, F., Jian, J., Yang, K., Jin, F. and Dou, S. *Nano Energy*, 2021, 81: 105601.

21. Gao, P., Ru, Q., Yan, H., Cheng, S., Liu, Y., Hou, X. and Chi-Chung Ling, F. *ChemElectroChem*, 2020, 7.1: 283-288.

22. Wu, F., Wang, Y., Ruan, P., Niu, X., Zheng, D., Xu, X. and Cao, X. *Mater. Today Energy*, 2021, 21: 100842.

23. Li, W., Gao, X., Chen, Z., Guo, R., Zou, G., Hou, H. and Zhao, J. *J. Chem. Eng.*, 2020, 402: 125509.

24. Zhang, N., Cheng, F., Liu, Y., Zhao, Q., Lei, K., Chen, C. and Chen, J. *J. Am. Chem. Soc.*, 2016, 138.39: 12894-12901.

25. Hao, J., Mou, J., Zhang, J., Dong, L., Liu, W., Xu, C. and Kang, F. *Electrochim. Acta*, 2018, 259: 170-178.

26. R. Tran, Z. Xu, B. Radhakrishnan, D. Winston, W. Sun, K. A. Persson and S. P. Ong, *Sci. Data*, 2016, **3**, 160080.

27. http://crystalium.materialsvirtuallab.org/ accessed on 18 March 2024

28. Vander Voort, G. F. (1999). Metallography, principles and practice. ASM international.